Suppression of DC Current Injection in Transformerless Grid Connected Inverters using a DC Link Current Sensing Approach

Abstract — There **is increasing interest in the use of transformer-less systems for grid connected photovoltaic applications. Compared to transformer coupled solutions, transformer-less systems offer a typical efficiency increase of 1-2%, reduced system size and weight, and a reduction in cost. However, the removal of the transformer has technical implications. In addition to the loss of galvanic isolation, dc current injection into the grid is a potential risk. Whilst desirable, complete mitigation of dc current injection via convention current control methods is known to be particularly challenging. For this reason, this paper proposes an active dc suppression method, in which the dc current injection is accurately determined by extracting the line frequency component from inverter dc link current measurements and then mitigated with an active closed loop controller. Experimental results from a laboratory grid connected inverter system are presented to demonstrate the high performance of the proposed technique.**

***Key Words*—Transformer-less, Grid Connected, Power Quality, Power Converters, DC Injection Suppression.**

I. INTRODUCTION

IN recent years, an increasing number of small-scale photovoltaic systems have been connected to the distribution network. At the heart of these low-power systems is a high efficiency power electronic converter that typically injects unity power factor current into the grid. Many conventional power converters are coupled to the grid using a line frequency transformer, which is large, heavy, and costly. Alternative topologies have been developed to enable the use of smaller, lower cost, high frequency transformers. Furthermore, in recent times, new promising topologies and control methods have been implemented to facilitate less bulky, cost effective, transformer-less solutions [1-3].

Unfortunately, without galvanic isolation, there are several well understood technical and safety issues to consider. Among these issues, the risk of dc current injection flowing into the network remains a potential concern [3-5]. Dc current injection may arise via the accumulation of several causes including non-ideal semiconductor device characteristics, asymmetries in switching behavior, gate drive circuit delays; small dc bias in current reference signals, quantisation errors in digital systems, and non-linearity and offset drift in typical Hall effect transducers [5-7]. Whilst dc current injection from an individual

inverter may be very small, the accumulative effect from multiple inverter installations can potentially saturate local distribution

transformers, adversely affect the normal load operation, and degrade power cables over time [5],[6],[8]. As a result, strict national guidelines and recommendations are normally in place to limit the dc current injection of an individual inverter unit [9]. A typical limit is 0.5% of the full load rated current. However, dc injection within these norms can still produce 50% larger excitation current in the distribution transformer [10]. Much research has been proposed to mitigate, or suppress, dc current injection at an individual inverter level. Broadly speaking, literature shows these solutions fall into the following four categories: i) sensor calibration techniques; ii) passive removal of dc current injection; iii) active dc suppression techniques; iv) advanced software solutions.

A typical sensor calibration method is proposed in [6],[11]. Here, an auto-calibration technique is presented to compensate for offset drift and nonlinearity in the current transducer. Due to the large inverter current controller gain at low frequencies, effective suppression of the dc injection is demonstrated. However, the calibration process requires double the sampling rate and the method is only effective for limited topologies and dc sources. With regards to passive cancellation approaches, a series dc blocking capacitor approach is common. This is only inherent in particular inverter topologies, for example the half-bridge inverter. However, these converters are not necessarily the optimal choice in grid connected applications. For this reason in many commonly selected topologies, such as the H-bridge, an electrolytic capacitor circuit can be placed between the inverter output and the point of common coupling [12]. Polarized electrolytic capacitors are not a desirable choice given the ac output of the inverter, however, they provide the necessary high capacitance value and voltage ratings. Given this, a polarity protection circuit is often included to preserve the integrity of the capacitors. More recently, attention has focused on active dc suppression techniques. Here, the dc current injection is directly measured, or indirectly estimated, via appropriate sensing and measurement techniques. Along with a dedicated control algorithm, the measurement feedback is utilized to actively compensate the dc current component. For example, the authors in [13] introduce a direct dc measurement technique based on a simple magnetic circuit composed of a magnetic core and compensation winding. Although this structure reduces the ac flux component without influencing the dc flux, the performance of dc the measurement relies greatly on the compensation winding, furthermore the dc current determination from the combined flux measurements is a non-trivial task. In [14], a 1:1 coupled inductor combined with a small-range current sensor is utilized to measure the dc current directly. However, this technique requires an extra sensor set combined with a specially designed coupled-inductor to achieve robust performance. Other approaches have discussed indirect dc current estimation by sensing the dc voltage offset introduced by the low pass filter ESR and dc current injection. Authors in [15] investigate a solution using a small 1:1 voltage transformer and an RC circuit to detect the dc offset voltage; however, complete removal of the dominant ac voltage component is difficult to achieve considering the phase shift between the grid voltage and the inverter output; hence acquiring an accurate dc voltage measurement is challenging. As a result, Ahfock and Bowetell in [16] introduce a double-stage RC circuit connected across the ripple filter. However, the small dc voltage offset detected is prone to noise. In addition, there are high common-mode voltage problems to consider. In [17] a dc suppression loop is proposed. Here, the dc voltage offset is measured at the inverter output via

a differential amplifier and a low-pass filter. This effectively resolves common-mode voltage problems, but the step-down offset voltage from the differential amplifier introduces accurate measurement challenges. Other state-of-the art solutions have been investigated using non-linear reactors [7],[18]. Typically, these schemes offer precision sensing but are very sensitive to the reactor design, and rely on sophisticated control solutions.

Unlike all aforementioned measurement techniques, active software solutions attempt to obtain the dc component from existing control feedback measurement signals. Generally, a major advantage is avoiding the need for additional hardware. Several techniques have been investigated in literature, all of which attempt to measure, or mitigate the dc injection. A real-time dc current measurement technique is proposed using double integration of the output current, building upon this, Guo et al. in [19] use the double integrator output within a feedback loop to compensate dc current injection. From a control perspective, this feedback loop acts as a software equivalent to the series blocking capacitor approach; hence it is often referred to as virtual capacitor concept. The major concern of the virtual capacitor approach is the accuracy of the current sensing circuit. If the sensor operating point drifts or the dc injection is not correctly sensed, the feedback control is likely to offer poor performance. The authors in [20] introduced an indirect dc estimation based on the software extraction of the dc link line-frequency voltage. As the dc link capacitor voltage is already sensed within the inverter system, no extra hardware is needed. However, owing to the minimal line-frequency voltage ripple (millivolts scale) on the dc link capacitor, accurate measurement of this ripple component which is superimposed onto a much larger dc voltage is challenging; any inaccuracy in the measurement ultimately results in degraded dc mitigation performance.

As mainstream literature continues to show, dc component mitigation is a challenging problem in grid connected inverter applications. For this reason, this paper introduces a novel dc suppression approach for single-phase grid connected transformer-less full-bridge inverters based on dc link current measurements. The dc current is extracted from the dc link current waveform and suppressed via an active control loop. Furthermore, fundamental ac current control is simultaneously implemented using the same dc link current measurement, thus eliminating the need for a conventional output current sensor.

II. DC Injection Analysis

This study focuses on a unipolar PWM switched transformer-less H-bridge inverter; a well understand and widely adopted topology for single phase PV applications due to its relatively small output filter requirements (Fig. 1). The four key switching states for the H-Bridge are listed in Table 1; states 1&2 are referred to as conducting states, states 3&4 are referred to as freewheeling states. The H-bridge inverter can be modelled using a switching function $S(t)$ which mathematically relates the dc input to the ac output, as shown in Fig.2. Neglecting high-frequency components, the line frequency representation of $S(t)$ is [20]:

$$S(t) = M_i sin(\omega t + \varphi_1) \quad (1)$$

M_i is the modulation index, ω is the fundamental frequency of the grid and φ_1 is the phase difference with respect to the grid voltage. From this, and with reference to Fig.2, the following voltage and current can be expressed:

$$V_{out}(t) = V_{dc}S(t) = V_{dc}M_i sin(\omega t + \varphi_1) \quad (2)$$

$$I_{dclink}(t) = I_g S(t) = I_g M_i sin(\omega t + \varphi_1) \quad (3)$$

As in most transformer-less applications, the inverter output current normally contains a fundamental ac component and dc component. This can simply be expressed as:

$$I_g(t) = I_{AC} sin(\omega t + \varphi_2) + I_{DC} \quad (4)$$

In (4), I_{DC} is the magnitude of the dc current injection, I_{AC} is the magnitude of ac output current, φ_2 is the phase difference with respect to the grid voltage. Substituting (4) into (3) yields:

$$I_{dcLink}(t) = [I_{AC} sin(\omega t + \varphi_2) + I_{DC}]M_i sin(\omega t + \varphi_1) \quad (5)$$

As described in (6), the dc and second harmonic component of the dc link current are determined by ac component and phase angles, whilst the line frequency component is solely introduced by dc injection. Assuming neglectable filter phase shift and unity power factor operation $\varphi_1 = \varphi_2 = 0$. In this case, it can be shown that:

$$I_{dcLink}(t) = \frac{M_i I_{AC}}{2}[1 - \cos(2\omega t)] + I_{DC}M_i sin(\omega t) \quad (7)$$

Equation (7) shows that the inverter ac output current results in the second harmonic component of the dc link current. Furthermore, it shows that the dc current component in the inverter output results in a fundamental frequency component in the dc link current. Thus, importantly, accurate measurement and extraction of the fundamental of the line-frequency component in the dc link facilitates determination of the dc component in the inverter output.

$$I_{dcLink}(t) = \frac{M_i I_{AC}}{2}[(1 - cos2\omega t)cos\varphi_1 cos\varphi_2 + sin2\omega t(sin\varphi_1 cos\varphi_2 + sin\varphi_2 cos\varphi_1) + (1 + cos2\omega t)sin\varphi_1 sin\varphi_2]$$

$$+I_{DC}\, M_i\, sin(\omega t + \varphi_1) \quad (6)$$

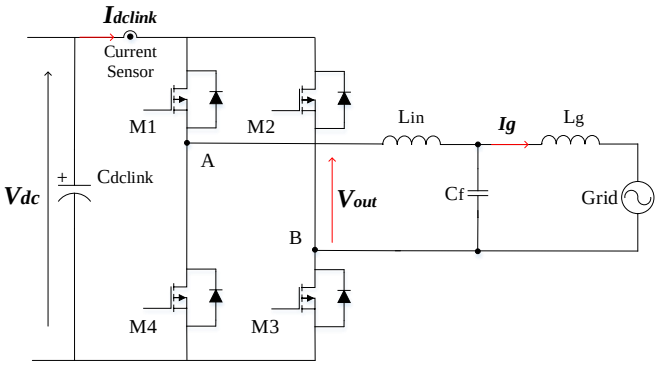

Fig. 1. Typical transformer-less H-bridge inverter with dc link sensor

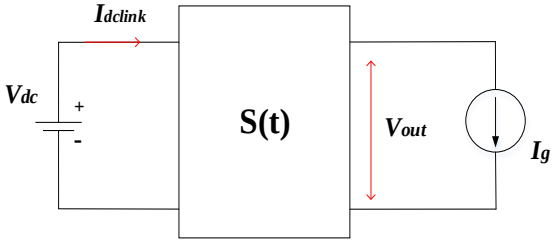

Fig. 2. Simplified model of the H-bridge

TABLE I

UNIPOLAR SWITCHED H-BRIDGE WORKING STATES

State	Switches States				V_{out}	I_{dclink}
	M1	M2	M3	M4		
1	On	Off	On	Off	V_{dc}	I_g
2	Off	On	Off	On	$-V_{dc}$	$-I_g$
3	On	Off	Off	On	0	0
4	Off	On	On	Off	0	0

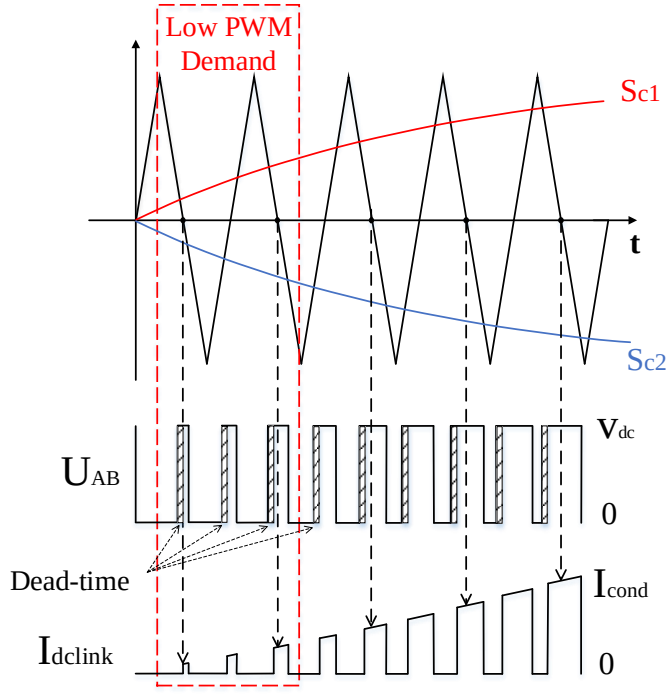

Fig. 3. Conducting sample of dc link current measurement

A. Analysis of Conducting Sampling with Dead-time Effect

As shown in Table I, in a unipolar switched H-bridge inverter, the dc link current has the same magnitude as the output current during a conducting state, whilst there is no current in the dc link during a freewheeling state. Consequently, the dc link current is made up of a train of PWM related current pulses. Previous studies have proven that, without over-modulation, the freewheeling measurement and conducting measurement can be separately determined by sampling at the peak or zero-crossing point of the modulating triangular carrier [6]. Therefore, the peak sampling utilized in conventional current control results in a series of zero measurements. To fully preserve knowledge of the dc link current, the samples have to be taken at the point where the triangular modulation signal crosses zero. Deadtime clearly has to be inserted between the required switching edges. Although it is a small amount of time depending on the characteristic of the switches, it reduces the duration of the conducting states as shown in Fig. 3. At low PWM demands, where the conducting pulses are narrow, the deadtime can eliminate the conducting pulses, or result in a zero-state measurement. Fortunately, as few PWM pulses are affected, the impact is limited. The reduction in conducting period introduced by deadtime can be calculated as:

$$P_{red} = \frac{t_d}{T} = t_d f_s \qquad (8)$$

For a 20 kHz switching frequency with a deadtime of 500 ns, the duty cycle reduction is 1% in each pulse.

B. DC Injection in Conducting DC Link Current

When operating at unity power factor (PF), the dc link conducting measurement is equal to the absolute inverter output current as shown in Fig. 4. Considering potential dc current injection, the conducting dc link current can be expressed as:

$$I_{Cond}(t) = \left|I_g(t)\right| = \left|I_{AC} sin\omega t + I_{DC}\right| \qquad (9)$$

Depending on the polarity of the conducting state, dc injection is observed as a square wave and offsets the conducting dc link current as shown in Fig. 4. The frequency spectrum of the dc link current is determined via Fourier analysis, as defined in (10).

$$I_{Cond}(t) = \underbrace{\frac{4I_{AC}}{\pi}\left(\frac{1}{2} - \sum_{n=1}^{\infty}\frac{1}{4n^2-1}cos2n\omega t\right)}_{Even\ Harmonics} + \underbrace{\sum_{n=1}^{\infty}\frac{4I_{DC}}{(2n-1)\pi}sin[(2n-1)\omega t]}_{Odd\ Harmonics}\ (n = 1,2,3\ldots) \qquad (10)$$

From (10), it can be seen that the even harmonics in the dc link current waveform are attributed to the fundamental ac component, whilst the odd harmonics are attributed to the dc current injection component in the system. Simplification of (10) is achieved by considering the impact on the line frequency ripple only (*n* equal to 1.) Thus:

$$I_{Cond}(t) = \frac{2I_{AC}}{\pi} - \frac{4I_{AC}}{3\pi}cos2\omega t + \frac{4I_{DC}}{\pi}sin\omega t \qquad (11)$$

Comparing with (7), the line frequency component is proportional to the dc current injection as described in (11). However, the magnitude of the line frequency component is now greater compared to (7), assuming $M_i < 1$. Therefore, the ability to extract the dc component accurately is improved.

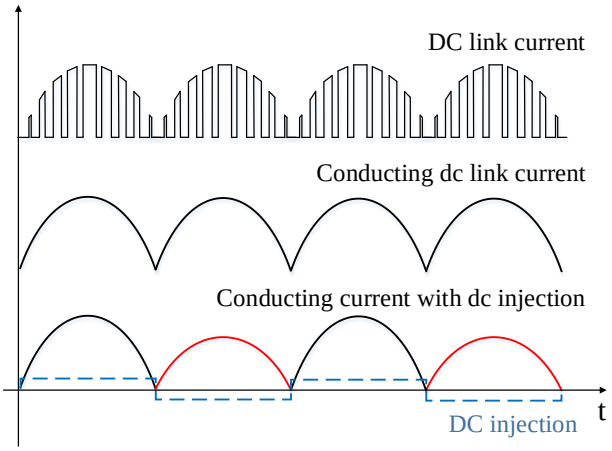

Fig. 4. Conducting current at unity power factor

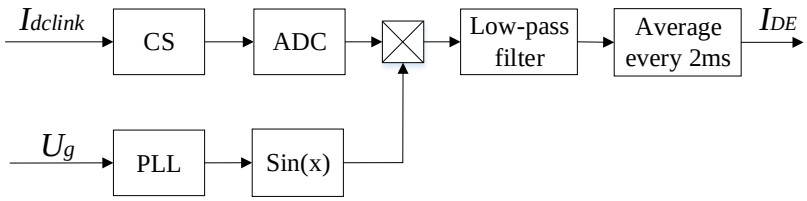

Fig. 5. Block diagram of the proposed extraction

III. Proposed DC Suppression Approach

The proposed dc suppression approach is shown in Fig. 5. The approach is based on digitally sampling the dc link current from current sensor (CS) during conducting periods. For a grid connected inverter system, a phase-locked loop (PLL) is generally utilized to provide synchronization with the grid. The output of the PLL is utilized by the proposed scheme for phase detection. Based on the aforementioned Fourier signal analysis technique, the line frequency of the conducting current is obtained by multiplying with a sine function at the same fundamental frequency.

$$I_{Ex}(t) = I_{Cond}(t) sin\omega t \qquad (12)$$

Then, through substituting I_{Cond} by (11), the frequency components of I_{Ex} can be expressed as:

$$I_{Ex}(t) = \frac{2I_{AC}}{\pi} sin\omega t - \frac{4I_{AC}}{3\pi}\cos 2\omega t sin\omega t - \frac{2I_{DC}}{\pi}\cos 2\omega t + \frac{2I_{DC}}{\pi} \qquad (13)$$

As described in (13), I_{DC} can now be determined from a dc quantity, rather than the line frequency component in (11). For the

purposes of dc extraction, the remaining ac quantities are redundant and they can be removed using a digital low-pass filter. As a practical point, owing to the narrow frequency range between the low-frequency ac polynomials and dc quantity, a low cut-off frequency (< 1 Hz) is required to effectively isolate the dc component. To improve that, an averaging algorithm is implemented following the filter, as shown in Fig. 5. This is required to remove the high frequency terms first expressed in (10), which reflects the complete characteristic behavior of the dc link conducting current. The averaging algorithm is simple to implement, and also relieves some of the burden on the low pass filter. With the combination of low-pass filter and average algorithm, the dc injection can be accurately determined from the resulting dc component at the output:

$$I_{DE} = \frac{2}{\pi} I_{DC} \qquad (14)$$

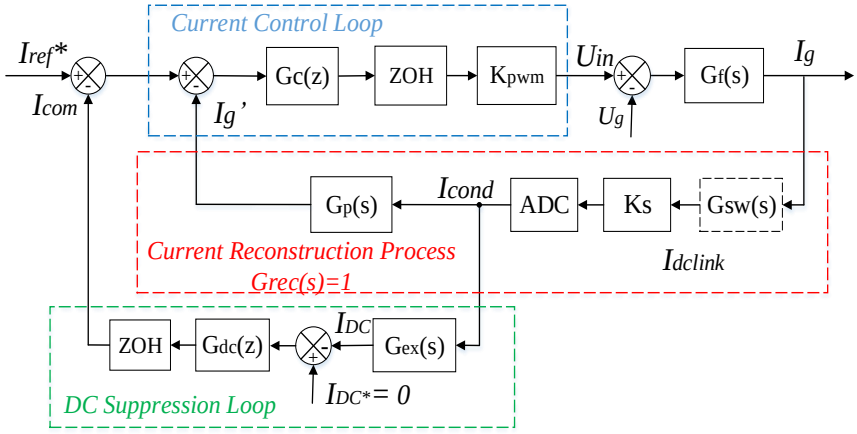

Fig. 8. DC link sensing approach with dc suppression control

The frequency components in (13) are derived from the fundamental frequency of conducting current only. As described in (10), the conducting current contains a wide range of frequency components, the frequency response of the proposed approach is analyzed to validate the extraction of the line frequency component.

A. Analysis of Frequency Response of Extraction

The control diagram for the proposed dc determination scheme is shown in Fig.6. As the line frequency component of the conducting current is obtained via multiplying by a fundamental frequency sine function, this process can be expressed as an s-domain transfer function (15), in which ω_0 is the fundamental frequency of the grid.

$$G_{sin}(s) = \frac{\omega_0}{s^2 + {\omega_0}^2} \qquad (15)$$

$G_{sin}(s)$ provides infinite gain at frequency ω_0 with greater attenuation at high frequencies [21],[22]. A first order low-pass filter $G_f(s)$ $(\omega_c/(s+\omega_c))$, where ω_c is the cut-off frequency, and averaging, $G_{avg}(s)$, is then applied to further eliminate the high-

frequency components. The averaging process can be expressed as a sliding window integration, where T is the averaging period.

$$y(t) = \frac{1}{T}\int_{t-T}^{t} u(\tau)dt = \frac{1}{T}\left[\int_{0}^{t} u(\tau)dt - \int_{0}^{t-T} u(\tau)dt\right] \quad (16)$$

Based on (16), the s-domain representation of the averaging can be derived as (17).

$$G_{avg}(s) = \frac{Y(s)}{U(s)} = \frac{1 - e^{-sT}}{sT} \quad (17)$$

Significant attenuation is found at each integer harmonic of fundamental frequency, $n\omega_0$. This is because the output of the average filter is effectively zero for periodic signals (e.g. sin and cos). Given (17), the transfer function of the proposed line frequency extraction process can be expressed as:

$$G_{ex}(s) = \frac{I_{DC}(s)}{I_{Cond}(s)} = \frac{\frac{1}{T}\omega_0\omega_c(1 - e^{-sT})}{s^4 + \omega_c s^3 + {\omega_0}^2 s^2 + {\omega_0}^2\omega_c s} \quad (18)$$

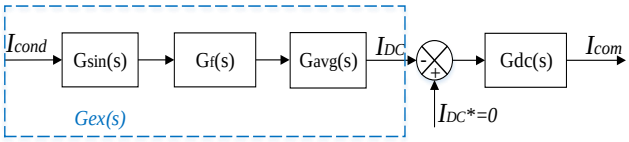

Fig. 6. Control diagram of the dc suppression loop

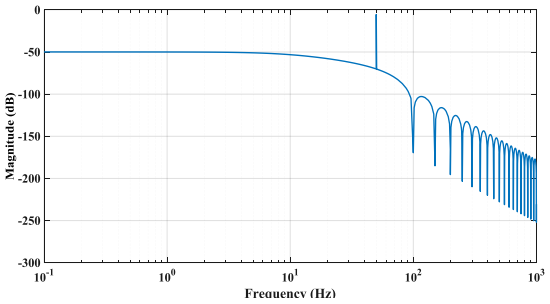

Fig. 7. Frequency response of the line frequency extraction

IV. Analysis of DC Link Current Control and Suppression

Generally, a conventional single phase grid-connected inverter system is controlled using inverter output current measurements. However, for the proposed dc suppression approach, a current sensor must be placed in the dc link. The use of two current sensors is undesirable increases the cost and complexity of the system. As the conducting dc link current used for dc suppression has the same magnitude of the output current, a simple reconstruction can be carried out to restore the output current digitally, eliminating the need for the conventional output current sensor. The output current control loop is then implemented as per a conventional

inverter. The control diagram of the dc link sensing technique, including current reconstruction and dc suppression, is shown in Fig. 8.

A. Current Control and DC Suppression based on DC Link Sensing Technique

Through the aforementioned conducting dc link sampling, the magnitude of the inverter output current is known. However, knowledge of the polarity is required to fully restore the output current waveform digitally. As reported in [6] the PWM index can be used to determine the polarity information. With positive PWM demand, the polarity of the conducting dc link current is the same as the inverter output current. For negative PWM demand, the conducting dc link current polarity is the opposite of the inverter output current. In this case, the output current is obtained by inverting the conducting dc link current measurement. The reconstruction process is shown in Fig. 8, where $G_{sw}(s)$ and $G_p(s)$ represent the switching function and polarity information from the PWM unit respectively. Following this procedure, provided the current waveform is obtained accurately, the transfer function of the current reconstruction may be expressed as:

$$G_{rec}(s) = \frac{I_g{}'(s)}{I_g(s)} = 1 \qquad (19)$$

With the output current available from the reconstruction, a conventional current loop is implemented where, as shown in Fig. 8, $G_c(z)$ is a typical PI or PR controller. As described in (20), K_{pwm} is the PWM gain, $G_f(s)$ is the output filter transfer function, T_s is the sample time. $I_{ref}(s)$ is the sinusoidal current demand and $I_{com}(s)$ is the compensation current from the dc suppression loop. By using a PR controller, the gain of $G_c(z)$ at fundamental frequency is very large. Therefore, the effect of the grid voltage $U_g(s)$ can be neglected. As such;

$$I_g(s) = \frac{G_c(z)\, e^{-sT_s}\, K_{pwm} G_f(s) \left[I_{ref}(s) - I_{com}(s)\right] + G_f(s)\, U_g(s)}{1 + G_c(z)\, e^{-sT_s}\, K_{pwm}\, G_f(s)} \qquad (20)$$

As described in (21), the proposed technique is capable of injecting ac current into the grid with compensating any dc current injection in the system.

$$I_g(s) = \frac{G_c(z) e^{-sT_s} K_{pwm} G_f(s)}{1 + G_c(z) e^{-sT_s} K_{pwm} G_f(s)} \left[I_{ref}(s) - I_{com}(s)\right] \qquad (21)$$

B. Analysis of the Offset in Current Sensor and Conditioning Circuit

In convention output current control, the undesirable offset of the current sensor and the signal conditioning circuit contributes an undefined dc measurement error in the controller, which ultimately has an impact on the dc injection. In dc link current sensing control, the measurement offset is defined as $\Delta \boldsymbol{I_{offset}}$, and thus the dc link current can be presented as:

$$I_{dcLink}(t) = \frac{M_i I_{AC}}{2}[1 - \cos(2\omega t)] + I_{DC} M_i sin(\omega t) + \boldsymbol{\Delta I_{offset}} \quad (22)$$

It can be seen that this offset introduces a dc component to the dc link current measurement, whilst the dc injection I_{DC} at output is related only to the line frequency component of dc link current. Therefore, unlike conventional output current control, offset of the current sensor and signal conditioning circuit will not contribute to any dc injection to the system. Moreover, with appropriate sensor calibration [6], ΔI_{offset} can be minimized to a point where it can to all intents and purposes be neglected.

C. Analysis of DC Determination Sensitivity

With the proposed line frequency component extraction from dc link current waveform in (14), the sensitivity of the dc current measurement can be quantified as:

$$S_c = \frac{I_{DE}}{I_{dclink}} \quad (23)$$

As stated, the dc link current I_{dclink} has the same amplitude as current I_{AC}. For a 2 kW PV system with an output current I_{AC} = 11.8 A and dc component injection of I_{DC} = 50 mA, the sensitivity of the dc link sensing technique is equal to:

$$S_c = \frac{\frac{2}{\pi} I_{DC}}{I_{AC}} = 2.7 \ \frac{mA}{A} \quad (24)$$

Compared to [20], where the line-frequency dc link voltage $V_{dclinkLFripple}$ is utilized for determining the dc current injection, the sensitivity S_D is calculated as:

$$S_D = \frac{V_{dclinkLFripple}}{V_{dclink}} \quad (25)$$

Assuming the dc link voltage ripple is precisely sensed and extracted, with grid frequency ω_g= 50 Hz, dc link capacitor C_{dclink} = 2200 μF and dc link voltage V_{dclink} = 400 V, the sensitivity of the approach S_D can also be calculated assuming the same dc current injection of 50 mA:

$$S_D = \frac{\frac{I_{DC}}{j\omega_g C_{dclink}}}{V_{dclink}} = 0.18 \ \frac{mV}{V} \quad (26)$$

Comparing (24) with (26), it is clear the dc link current sensing technique improves the dc measurement sensitivity compared to the dc link voltage feedback approach. As the output current restoration process eliminates the need for an output current sensor, the technique is still recognized as a control-based solution; however, no extra hardware is needed.

Fig. 9. H-bridge inverter with dc link current sensor

TABLE II

EXPERIMENTAL PARAMETERS

Symbol	Quantity	Value(Unit)
V_{dc}	DC Link Voltage	120 (V)
V_g	Grid Voltage RMS	60 (V)
I_g	Output Current	7.0 (A)
L_{in}	Inverter Side Inductor	0.8 (mH)
L_g	Grid Side Inductor	0.3 (mH)
C_f	Filter Capacitor	10 (μF)
f_{sw}	Switching Frequency	20 (kHz)
f_c	Cut-off Frequency of External Measurement Circuit	0.35 (Hz)

V. EXPERIMENTAL VALIDATION

An experimental prototype grid-connected H-bridge inverter system with dc link current sensor is implemented (Fig. 9). The inverter is controlled by a Texas Instruments™ TMS320F28377D DSP. The experimental inverter is operated with a 20 kHz unipolar PWM switching scheme. An LCL filter is connected to the inverter output to attenuate high-frequency harmonics. Key system parameters are presented in Table II. For comparison purposes only, a current sensor is placed at the inverter output for conventional output current control. In addition, a 0.1 Ω shunt resistor is inserted into the inverter output path. A low-pass RC filter (0.35 Hz cut-off frequency) is connected across the shunt to monitor the dc current injection.

The inverter is controlled via a PR controller with proportional gain $K_p = 0.15$, resonant gain $K_r = 180$ and the bandwidth

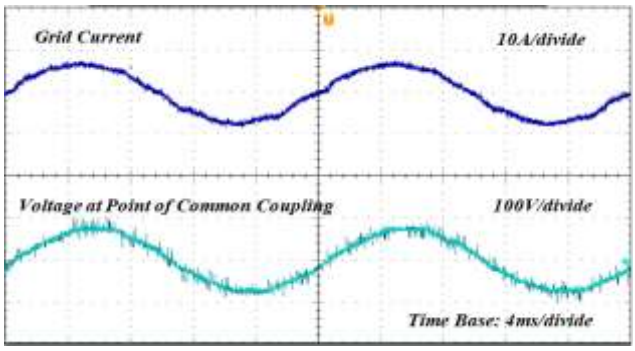

Fig. 10. Unity power factor operation of dc link current control

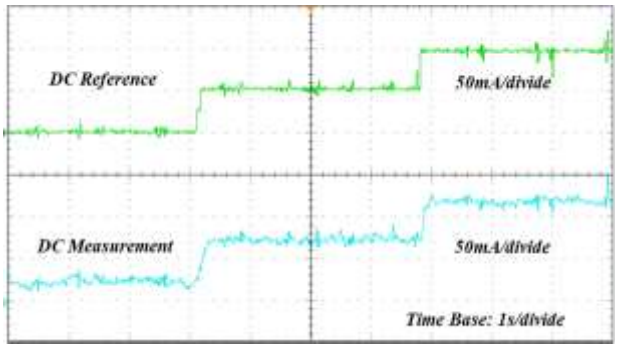

Fig. 13. DC determination with pre-determined reference

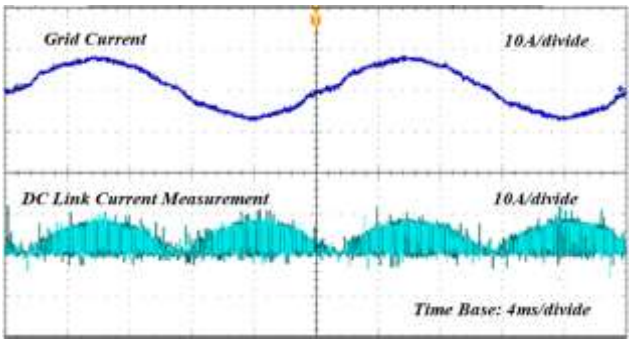

Fig. 11. DC Link current measurement over two cycles

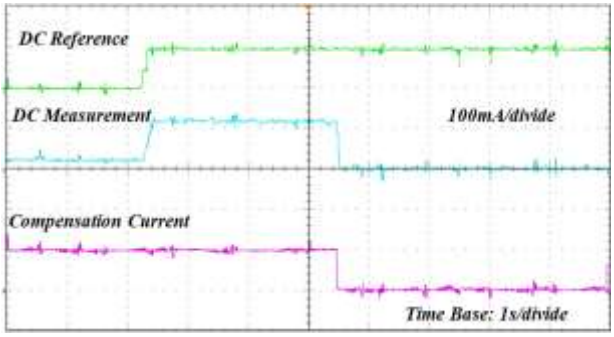

Fig. 14. DC measurement with suppression enabled

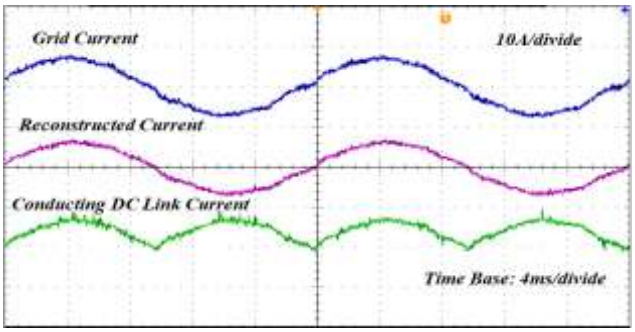

Fig. 12. Post-processed current measurements

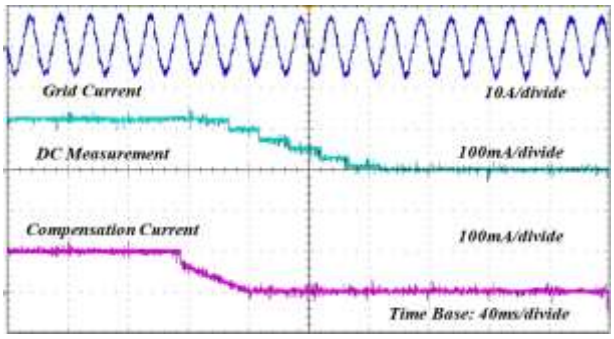

Fig. 15. Dynamic transient of dc suppression

$\omega_c = 5\,rad/s$, with a given current reference of 7.0 A, Fig. 10 shows the inverter operation at unity power factor with respect to grid voltage. As the controller is implemented with dc link current, the dc link current sensor measurement is presented in Fig. 11, which is a series of positive PWM current pulses. For comparison purposes, through the use of digital-to-analogue converter, Fig. 12 shows the conducting current and software-reconstructed output current in the microprocessor. With 20 kHz sampling, the conducting dc link current waveform obtained is the mathematical absolute of output current, and the output current reconstructed from it performs identically with the output current measurement achieved from output current sensor. Validation at non-unity power factor is also confirmed when the inverter operates at a power factor of 0.9. Unlike unity power factor, the dc link current waveform exhibits periods of negative magnitude pulses, which are measured during the conducting current period. However, from the control perspective, this is not an issue. The polarity of the PWM demand is reversed during this period, hence

reconstruction is not affected.

With the conducting dc link current and grid phase information accessible from previous current control, the dc injection can be accurately determined from proposed technique. To validate the dc measurement process, a deliberate predetermined dc component is introduced by superimposing a dc bias onto the current reference [17]. Fig. 13 shows the introduced dc bias and the extracted dc current measurement using the proposed technique. Initially, without introducing any dc current, the measured dc injection is confirmed as 25 mA. Then, a 50 mA step change bias signal is injected into the dc reference at 3.1s, followed by a further 50 mA step at 6.8 s. As shown in Fig. 13, the dc injection is rapidly and accurately extracted by the proposed measurement scheme. The steady state dc current measurements are confirmed as 75 mA and 125 mA; matching the measurements from the external dc measurement circuit. As such, dc component determination is validated.

As the dc suppression is carried out based on the real-time dc current measurement, Fig. 14 shows the compensated dc measurement when enabling the proposed closed loop suppression approach. Here, a 100 mA dc bias is added to the current reference. Through enabling the dc suppression loop at 5.5 s, an inverse compensation current (-120 mA) is produced, which counteracts the dc injection in the system. As shown in Fig. 14, although the 100 mA dc reference still exists, the dc measurement falls back to zero when the suppression loop is activated, thus confirming the effectiveness of the scheme.

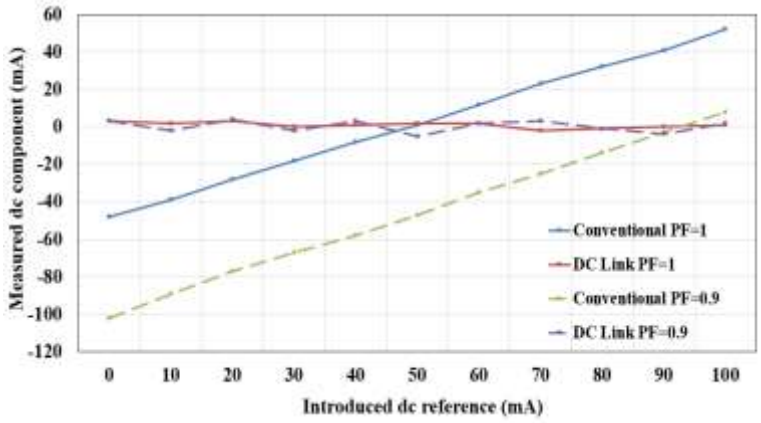

Fig. 16. Comparison of dc measurement at different PFs

The transient characteristics of the dc suppression approach is presented in Fig. 15, alongside the actual output current injected into the grid. When the dc suppression mechanism is enabled, the dc component is fully suppressed within 0.1 s demonstrating the real-time capabilities of the scheme. Meanwhile, even with significant step in dc current component, the output current remains robust and stable. Similar results have been achieved over a wide range of operating conditions. Fig. 16 shows the averaged dc measurements of conventional output current control and proposed dc link sensing approach when gradually increasing the dc bias into the reference at various power factors. For comparison, Fig. 16 also shows the results which have been obtained using conventional current control. It is clear the conventional current control is incapable of removing the dc injection, the dc

measurement varies from -100 mA to 50 mA; the dc injection is directly proportional to the bias signal imposed. However, with the dc link sensing and suppression approach, the averaged dc component is effectively limited to within 5 mA regardless of any dc current introduced. This performance is within the bounds of most international recommendations regarding dc current injection. Furthermore, recorded total harmonic distortion of 4.65% is also within acceptable limits [9].

VI. Conclusion

This paper presents an effective dc current suppression approach for single-phase transformer-less grid-connected full-bridge inverter system. Using a dc link current sensor, dc current injection is accurately measured by extracting the line frequency component of the dc link current waveform and then mitigated using an active dc current suppression loop. The output current reconstruction process permits closed loop current control via the dc link current sensor, thus eliminating the need for the conventional output current sensor. Full mathematical derivation and detailed analysis of the proposed dc suppression technique are presented in the paper. Experimental results validate the robust performance of the proposed scheme over a range of operating conditions. Overall, the approach presented is a high performance, cost-effective, control based solution for minimizing dc current injection in low power, single-phase, grid connected PV applications.

References

[1] D. Barater, G. Buticchi, A. S. Crinto, G. Franceschini, and E. Lorenzani, "Unipolar PWM strategy for transformerless PV grid-connected converters," *IEEE Transactions on Energy Conversion*, vol. 27, pp. 835-843, 2012.

[2] M. Armstrong, D. J. Atkinson, C. M. Johnson, and T. D. Abeyasekera, "Low order harmonic cancellation in a grid connected multiple inverter system via current control parameter randomization," *IEEE Transactions on Power Electronics*, vol. 20, pp. 885-892, 2005.

[3] S. V. Araújo, P. Zacharias, and R. Mallwitz, "Highly efficient single-phase transformerless inverters for grid-connected photovoltaic systems," *IEEE Transactions on Industrial Electronics*, vol. 57, pp. 3118-3128, 2010.

[4] Y. Yang, F. Blaabjerg, and H. Wang, "Low-voltage ride-through of single-phase transformerless photovoltaic inverters," *IEEE Transactions on Industry Applications*, vol. 50, pp. 1942-1952, 2014.

[5] Q. Yan, X. Wu, X. Yuan, Y. Geng, and Q. Zhang, "Minimization of the DC component in transformerless three-phase grid-connected photovoltaic inverters," *IEEE Transactions on Power Electronics*, vol. 30, pp. 3984-3997, 2015.

[6] M. Armstrong, D. J. Atkinson, C. M. Johnson, and T. D. Abeyasekera, "Auto-calibrating DC link current sensing technique for transformerless, grid connected, H-bridge inverter systems," *IEEE Transactions on Power Electronics*, vol. 21, pp. 1385-1393, 2006.

[7] G. Buticchi, E. Lorenzani, and G. Franceschini, "A DC offset current compensation strategy in transformerless grid-connected power converters," *IEEE Transactions on Power Delivery*, vol. 26, pp. 2743-2751, 2011.

[8] H. Jedtberg, A. Pigazo, M. Liserre, and G. Buticchi, "Analysis of the robustness of transformerless PV inverter topologies to the choice of power devices," *IEEE Transactions on Power Electronics*, vol. 32, pp. 5248-5257, 2017.

[9] I. Committee, "IEEE standard for interconnecting distributed resources with electric power systems," *New York, NY: Institute of Electrical and Electronics Engineers*, 2003.

[10] S. N. Vukosavić and L. S. Perić, "High-precision sensing of DC bias in AC grids," *IEEE Transactions on Power Delivery*, vol. 30, pp. 1179-1186, 2015.

[11] F. Berba, D. Atkinson, and M. Armstrong, "A new approach of prevention of DC current component in transformerless grid-connected PV inverter application," in *Power Electronics for Distributed Generation Systems (PEDG), 2014 IEEE 5th International Symposium on*, 2014, pp. 1-7.

[12] W. Blewitt, D. Atkinson, J. Kelly, and R. Lakin, "Approach to low-cost prevention of DC injection in transformerless grid connected inverters," *IET Power Electronics*, vol. 3, pp. 111-119, 2010.

[13] R. Nalepa, F. Grecki, M. Ostrogórska, P. Aloszko, and J. Duc, "DC-bias current measurement in high power AC grids," in *Power Electronics and Applications (EPE), 2013 15th European Conference on*, 2013, pp. 1-5.

[14] A. Abdelhakim, P. Mattavelli, D. Yang, and F. Blaabjerg, "Coupled-Inductor-Based DC Current Measurement Technique for Transformerless Grid-Tied Inverters," *IEEE Transactions on Power Electronics*, vol. 33, pp. 18-23, 2018.

[15] R. Sharma, "Removal of DC offset current from transformerless PV inverters connected to utility," in *Proceedings of the 40th International Universities Power Engineering Conference (UPEC 2005)*, 2005, pp. 1230-1234.

[16] L. Bowtell and A. Ahfock, "Direct current offset controller for transformerless single-phase photovoltaic grid-connected inverters," *IET Renewable Power Generation*, vol. 4, pp. 428-437, 2010.

[17] G. He, D. Xu, and M. Chen, "A novel control strategy of suppressing DC current injection to the grid for single-phase PV inverter," *IEEE Transactions on Power Electronics*, vol. 30, pp. 1266-1274, 2015.
[18] S. N. Vukosavić and L. S. Perić, "High-Precision Active Suppression of DC Bias in AC Grids by Grid-Connected Power Converters," *IEEE Transactions on Industrial Electronics*, vol. 64, pp. 857-865, 2017.
[19] G. Xiaoqiang, G. Herong, and S. Guocheng, "DC injection control for grid-connected inverters based on virtual capacitor concept," in *Electrical Machines and Systems, 2008. ICEMS 2008. International Conference on*, 2008, pp. 2327-2330.
[20] Y. Shi, B. Liu, and S. Duan, "Eliminating DC current injection in current-transformer-sensed STATCOMs," *IEEE transactions on Power Electronics*, vol. 28, pp. 3760-3767, 2013.
[21] H. Khalfalla, S. Ethni, M. Al-Greer, V. Pickert, and M. Armstrong, "An adaptive proportional resonant controller for single phase PV grid connected inverter based on band-pass filter technique," in *Compatibility, Power Electronics and Power Engineering (CPE-POWERENG), 2017 11th IEEE International Conference on*, 2017, pp. 436-441.
[22] R. Teodorescu, F. Blaabjerg, M. Liserre, and P. C. Loh, "Proportional-resonant controllers and filters for grid-connected voltage-source converters," *IEE Proceedings - Electric Power Applications*, vol. 153, pp. 750-762, 2006.

Weichi Zhang was born in Shaanxi, China, in 1990. He received the B.E degree in measurement and control technology from Xi'an University of Technology, Xi'an China, in 2012, and M.S. degree in automation and control from Newcastle University, Newcastle upon Tyne, U.K., in 2014. He is currently working toward the Ph.D. degree in electrical engineering at Newcastle University. His research interests include control of renewable energy systems, and power quality improvements of grid-connected applications.

Matthew Armstrong received the M.Eng. and Ph.D. degrees from Newcastle University, Newcastle Upon Tyne, U.K. in 1998 and 2006 respectively. He is currently Senior Lecturer and a member of the Electrical Power Group at Newcastle University. His current research interests include advanced control of grid connected renewable energy systems, real-time digital control of power electronic converters, Li-ion battery characterization, system identification\parameter estimation, and hardware in the loop emulation.

Mohammed A. Elgendy received the B.Sc. degree from Menoufia University, Menoufia, Egypt, in 1997; the M.Sc. degree from Ain Shams University, Cairo, Egypt, in 2003; and the Ph.D. degree from Newcastle University, Newcastle upon Tyne, U.K., in 2010, all in electrical engineering. From 1998 to 2006, he was a Research Assistant with the New and Renewable Energy Department, Desert Research Centre, Cairo, Egypt. From 2011 to 2014, he was a Research Associate with the Electrical Power Research Group, Newcastle University, where he currently holds the position of Lecturer. His research focus is on design and control of power electronic converters for drives and renewable generation schemes.